OPEN

Imaging Microscopic Features of Keratoconic Corneal Morphology

Kate Grieve, PhD,† Cristina Georgeon,* Felipe Andreiuolo, MD, PhD,* Marie Borderie,* Djida Ghoubay, MSc,*† Josette Rault,* and Vincent M. Borderie, MD, PhD*†*

Purpose: To search for gold-standard histology indicators using alternative imaging modalities in keratoconic corneas.

Methods: Prospective observational case–control study. Fourteen keratoconic corneas and 20 normal corneas (10 in vivo healthy subjects and 10 ex vivo donor corneas) were examined. Images of corneas were taken by spectral domain optical coherence tomography (SD-OCT) and in vivo confocal microscopy (IVCM) before keratoplasty. The same removed corneal buttons were imaged after keratoplasty with full-field optical coherence microscopy (FFOCM) and then fixed and sent for histology. Controls consisted of normal subjects imaged in vivo with IVCM and donor corneas imaged ex vivo with FFOCM. Corneal structural changes related to pathology were noted with each imaging modality. Cell density was quantified by manual cell counting.

Results: Keratoconus indicators (ie, epithelial thinning/thickening, cell shape changes, ferritin deposits, basement membrane anomalies, Bowman layer thinning, ruptures, interruptions, scarring, stromal modifications, and appearance of Vogt striae) were generally visible with all modalities. Additional features could be seen with FFOCM in comparison with gold-standard histology, particularly in the Bowman layer region, whereas the combination of SD-OCT plus IVCM detected 76% of those features detected in histology. Three-dimensional FFOCM imaging aided interpretation of two-dimensional IVCM and SD-OCT data. Basal epithelial cell and keratocyte densities were significantly lower in patients with keratoconus than those in normals ($P < 0.0001$).

Conclusions: Structural and cellular assessment of the keratoconic cornea by means of either in vivo SD-OCT combined with IVCM or ex vivo FFOCM in both cross-sectional and en face views can detect as many keratoconus indicators as gold-standard histology.

Received for publication March 29, 2016; revision received May 30, 2016; accepted June 24, 2016. Published online ahead of print August 25, 2016.

From the *Quinze-Vingts National Ophthalmology Hospital, Paris, France; and †Vision Institute/CIC, UPMC Université Paris, UMR_S/INSERM/CHNO des/CNRS, UMR, Paris, France.

Supported by the Agence Nationale de Recherche (ANR), under a PRTS (Projet de Recherche Translationelle en Santé) grant (ANR-13-PRTS-0009).

The authors have no conflicts of interest to disclose.

Reprints: Kate Grieve, PhD, Vision Institute, 17 rue Moreau, 75012 Paris, France (e-mail: kategrieve@gmail.com).

Key Words: imaging, cornea, keratoconus, optical coherence tomography, confocal microscopy

(*Cornea* 2016;35:1621–1630)

Keratoconus is a noninflammatory degenerative eye disorder that affects 1 in 2000 people worldwide, in which structural changes cause the cornea to thin and protrude in a conical shape.[1,2]

A typical clinical checkup for a patient with keratoconus includes slit-lamp examination and video topography (combining results from Placido and slit-lamp or Scheimpflug camera images, such as the Orbscan and Pentacam devices[3]). To approach a quasi-histological diagnosis, optical coherence tomography (OCT)[4,5] and in vivo confocal reflectance microscopy (IVCM)[6] have recently been demonstrated to aid in the diagnosis of keratoconus.

OCT,[7] most commonly in the spectral domain (SD-OCT), is widely used in ophthalmology. Image orientation is typically cross-sectional, and resolution is typically on the order of a few microns, permitting gross structural assessment of corneal disease but providing no cellular details. Ultrahigh-resolution OCT using a custom-built prototype achieved 1.1 μm axial resolution × 25 μm lateral resolution in the cornea, allowing measurement of Bowman layer (BL) thickness in keratoconic eyes.[8,9]

IVCM captures en face images of the cornea, providing information on cellular changes associated with corneal diseases thanks to its lateral resolution of 1 μm. Cross-sectional views are not currently available on commercial systems as en face slices are acquired manually one by one rather than automatically in stacks. Reconstruction of IVCM cross-sections has been demonstrated on a laboratory-modified setup,[10] with 1 μm lateral × 7.6 μm axial resolution.

Full-field optical coherence microscopy (FFOCM)[11,12] is a variant of conventional OCT in which two-dimensional en face images, similar to IVCM views, are captured on a camera and cross-sectional views can be extracted from the three-dimensional (3D) data sets that are obtained by scanning in the depth direction. This configuration allows for higher resolution than conventional OCT, on the order of 1 μm. FFOCM has been used to image ophthalmic tissues, including cornea,[13,14] limbus,[15] lens, and retina.[16]

The aim of this study was to assess keratoconus, normal subject, and donor corneas with a combination of en face images and cross-sections obtained with SD-OCT, IVCM, FFOCM, and gold-standard histology to discover the strength

of each technique by comparing the indicators visible with each. We thereby intend to propose which imaging technology or combination of technologies can provide structural information equal or superior to histology in clinical practice.

METHODS

Study Design and Ethics

This was a prospective observational case–control study. Informed consent was obtained from all patients. No modifications to French standards of treatment or follow-up were made. Institutional Review Board approval was obtained from the Patient Protection Committee, Ile-de-France V (14944). The study was conducted according to the tenets of the Declaration of Helsinki and followed international ethical requirements for human tissues.

Corneal Tissues

Characteristics of corneas and patients are shown in Table 1. Fourteen corneal buttons from 14 patients with keratoconus, 10 donor corneas, and 10 normal corneas from 10 healthy subjects were included in the study. All keratoconus corneas were at a sufficiently advanced stage to require keratoplasty. Keratoconic corneas were assessed with all imaging modalities, whereas donor corneas served as controls for ex vivo imaging modalities (FFOCM and histology), and corneas from healthy subjects served as controls for in vivo imaging modalities (SD-OCT and IVCM).

Pathological corneal buttons were obtained during keratoplasty procedures performed on patients at the Quinze-Vingts National Ophthalmology Hospital. They were collected from the operating room at the time of keratoplasty and conserved in the CorneaJet (EuroBio, France) medium during FFOCM imaging and then fixed in 4% formaldehyde before transfer to the pathology laboratory for histological processing.

Donor corneas were obtained from the tissue bank of the Etablissement Français du Sang, Ile-de-France (Paris, France) after they had passed the use-by date determined by French Eye Banking regulations. Donor stroma was inspected macroscopically and with light microscopy to assure the absence of any anomalies such as opacities.[17] The donor corneas were preserved in CorneaMax (EuroBio, Les Ulis, France) medium for a maximum of 35 days at 31°C, in accordance with European Eye Banking regulations. They were then placed in CorneaJet (EuroBio) medium containing dextran for deturgescence 48 hours before imaging.

Normal corneas from healthy subjects were used for cell density assessments with IVCM. Patients with keratoconus and healthy subjects were age matched (Table 1). This was important for cell density assessment as aging is associated with decreased cell density, in addition to reduced corneal thickness and increased corneal scatter.[18] Donor corneas were not age matched and so were not considered for cell density assessments.

Image Acquisition and Assessment Protocol

Care was taken to consistently image the same region of each cornea with each modality by keeping a visual record of images acquired and associating the same 3 authors (an orthoptist, an imaging expert, and a pathologist) with the chain of image acquisitions through different modalities to ensure continuity, that is author C.G. imaged with SD-OCT and IVCM, authors C.G. and K.G. imaged with FFOCM, and then authors K.G. and F.A. selected the corresponding histological slices. These same 3 authors then performed the image analysis, along with the input from 2 of the remaining authors who were not involved with the acquisition process.

In Vivo Assessment of Corneas

Specifications of imaging modalities are summarized in Table 2. The day before keratoplasty, patients were assessed in vivo with SD-OCT (RTVue-100; Optovue Inc, Fremont, CA) and IVCM (Heidelberg Retina Tomograph III; Heidelberg Engineering GmbH, Heidelberg, Germany). Normal corneas from healthy subjects were assessed in vivo with the same techniques. We acquired 6-mm wide SD-OCT scans centered on the conus and SD-OCT pachymetry maps, along with a series of 600 to 1600 en face IVCM images per patient, captured manually at nonautomated depth intervals by a skilled operator (author C.G., orthoptist), at the conus for keratoconus and at the center for normals, moving down through the depth of the cornea, paying particular attention to interesting features that seemed relevant to the pathology, and depending on good patient fixation for stability. Features noted in SD-OCT were located and matched in IVCM acquisitions by the same operator. The location of the conus was considered to be at the thinnest point on SD-OCT pachymetry maps. Axial × lateral resolution of SD-OCT was 5×8 μm,[19] and 7.6×1 μm for IVCM.[10,20]

Ex Vivo Assessment of Corneas

Full-Field Optical Coherence Microscopy

The FFOCM system used (LightCTScanner; LLTech, Paris, France) has been described previously.[13] Image stacks at the conus for keratoconus and at the center for normals were acquired on each button covering the entire corneal thickness, with an image acquired every micron in depth. Features noted in

TABLE 1. Characteristics of Corneas and Patients

	Keratoconus	Donors	Healthy Subjects
N	14	10	10
Patient or donor age, yrs	35 ± 16	71 ± 18	35 ± 18
Preservation time in the donor cornea storage medium	<1 h	>35 d	N/A
Imaging modalities	SD-OCT, IVCM, FFOCM, histology	FFOCM, histology	SD-OCT, IVCM

TABLE 2. Comparison of Different Imaging Modalities Used for Corneal Evaluation

Imaging Modality	SD-OCT	IVCM	FFOCM	Histology
Resolution (lateral × axial), μm	8 × 5	1 × 7.6	1.6 × 1	>0.2 × 4 typically
Field, μm	6 mm width × 2 mm depth	300 × 300	800 × 800 × 200–1000 depth	Whole sample down to zoomed detail, depending on objective and detector combination
Field orientation	Typically cross-section	En face	En face and cross-section	Typically cross-section
In vivo/in vitro (ie, excised tissue with live cells in culture)/ex vivo (ie, excised tissue without live cells)	In vivo	In vivo	In vitro	Ex vivo (formalin fixed paraffin embedded)
Tissue handling	None	Contact gel	Contact gel	Fixing, staining, and slicing
Intraocular pressure	Yes	Yes	No	No

SD-OCT and IVCM were located and matched in FFOCM acquisitions by the same operator. 3D image stacks could be examined in en face and cross-sectional views using multiplanar reconstruction software provided with the system.

Histology

After FFOCM assessment, the corneas were fixed (4% formaldehyde), and histological processing was performed in the histopathology laboratory. Hematoxylin and eosin stains (HESs) and periodic acid–Schiff stains were performed on paraffin-embedded material as these are routine stains for corneal pathology. To search for ferritin deposits, an additional stain of Perls' Prussian blue was performed. Photographs of histological slices were taken by 2 authors (an imaging expert and a pathologist), who located and matched the features noted in SD-OCT, IVCM, and FFOCM.

Comparison of Imaging Modalities

Images of each patient from all modalities were independently analyzed by 3 of the authors (an imaging expert, an orthoptist, and a pathologist), and a tally was made of features noted with each modality. The resulting tallies were reviewed, and an image-by-image, case-by-case analysis was performed as a group by those 3 authors who had undertaken the independent analyses, along with the additional input of a second orthoptist and an ophthalmologist. Therefore, for each particular feature of each particular case, 3 authors independently noted whether they detected this feature with each modality, and then 5 authors discussed whether each detection was considered valid. Any cases of discordance were eliminated. Qualitative descriptions of features are illustrated in Figures 1–3, and the tallies recorded are presented in Table 3, with totals expressed in number of features detected. Thus, we count the number of indicators detected with each modality and compare this with the number detected by gold-standard histology.

An additional parameter was investigated concerning artifactual tissue damage due to epithelial contact in the case of IVCM, tissue handling in FFOCM, and tissue processing for histology. Epithelial detachments and/or ruptures were tallied for each imaging modality for both pathological and normal corneas. We considered only epithelial detachment and/or rupture as being possibly due to contact or ex vivo artifacts as these were the only features that were never seen in vivo with SD-OCT.

Corneal Cell Density Assessment

As IVCM is capable of cellular resolution imaging in the in vivo cornea, we used IVCM images to quantify cell density in the keratoconic versus normal cornea. We chose to follow the IVCM convention of expressing cell density in terms of areal density, that is, in cells per square millimeter. Masked en face images obtained with IVCM were analyzed using FIJI image processing software (National Institutes of Health, Bethesda, MD). In stroma, images were inverted to enhance visibility of nuclei. After contrast enhancement, keratocyte nuclei were manually counted by 2 operators using the Fiji "cell counter" plugin (Kurt De Vos, University of Sheffield) to assess repeatability. Only bright and clear oval features were considered to be nuclei. Nuclei that landed on the border of the image were counted for only 2 of the 4 sides of the image. To reflect the differing keratocyte density on progression through the stroma from anterior to posterior, the corneal stroma was considered to be made up of 4 layers (very anterior, anterior, mid, and posterior), and 28 images were selected as follows: 3 images within the very anterior layer, 15 in the anterior layer, and 5 in mid and posterior layers. The very anterior stroma representing the first 2% of stromal thickness was analyzed separately from the anterior stroma because it featured very high keratocyte density in all the assessed corneas. The number of images per layer required for a reliable count was determined by stepwise analysis.[21] For the epithelium and endothelium, we counted cell centers rather than nuclei because of the regular appearance of the epithelial and endothelial cell mosaics with bright cell contours and dark centers with nonuniform visibility of nuclei. One image of each layer (ie, superficial, mid, and basal epithelial layers, and endothelium) was selected for each cornea.

Nerve Assessment

Branching and the mean thickness of nerves in the subbasal plexus and stroma were measured manually on IVCM images of n = 11 patients and n = 9 normals. In the remaining subjects of this study, nerves were not sufficiently visible for measurement. For each subject, one image was selected where the subbasal nerve plexus was most visible (at an average depth from the corneal surface of 35 ± 8 μm for normals and 43 ± 18 μm for keratoconus) and one where a stromal nerve was visible (at an average depth of 252 ± 93 μm for normals and

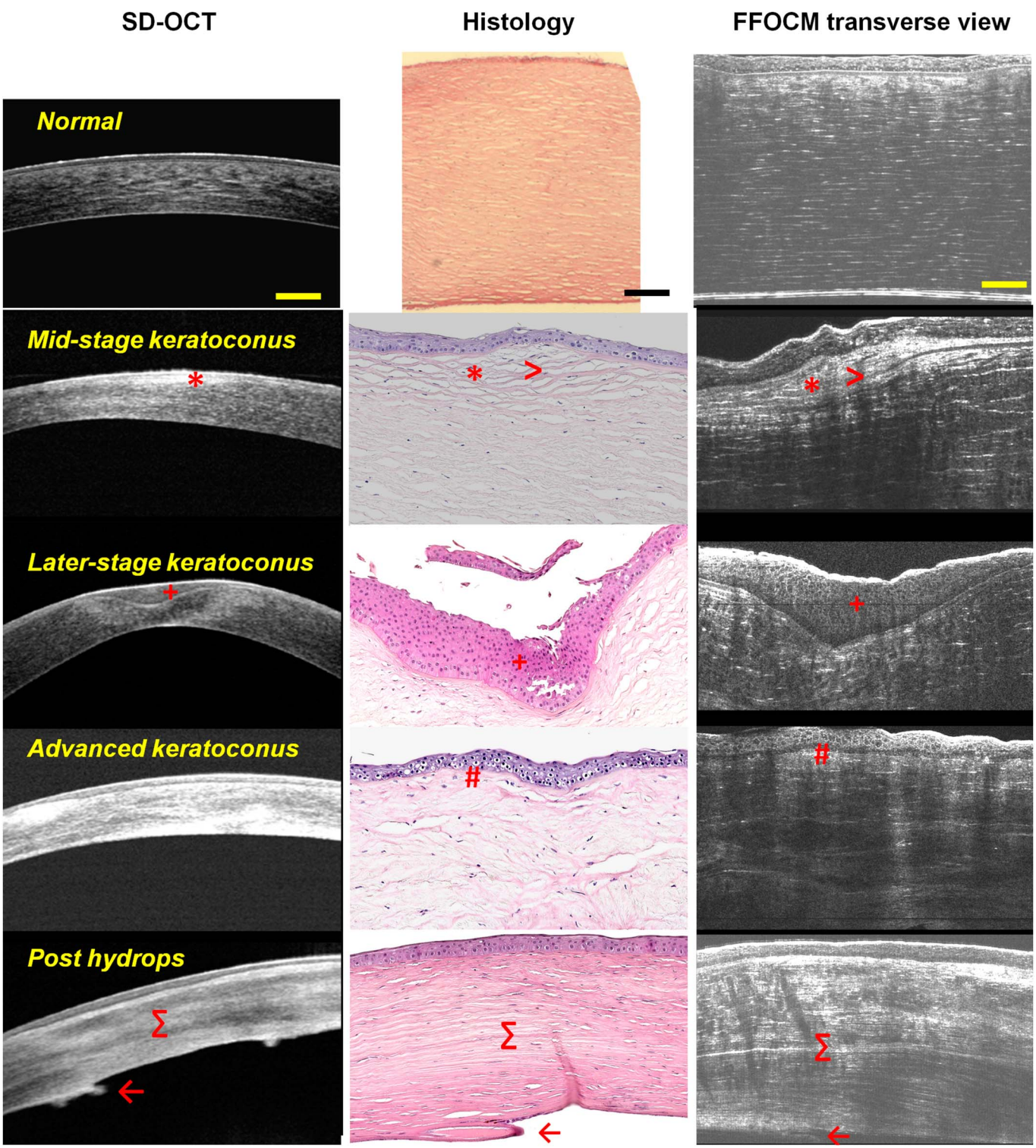

FIGURE 1. Cross-sectional views of the normal cornea and keratoconus. Scale bars 100 μm in FFOCM and histology, 200 μm in SD-OCT. The normal cornea and keratoconus in different patients at early to advanced stages (top to bottom rows) as viewed with SD-OCT (left column), histology (center column), and FFOCM in cross-section (right column panels). Indicators noted are as follows: >BL interruption; *fibrotic tissue; +thickened epithelium; #BL absent; ∑pan stromal scar; ←Descemet scarring.

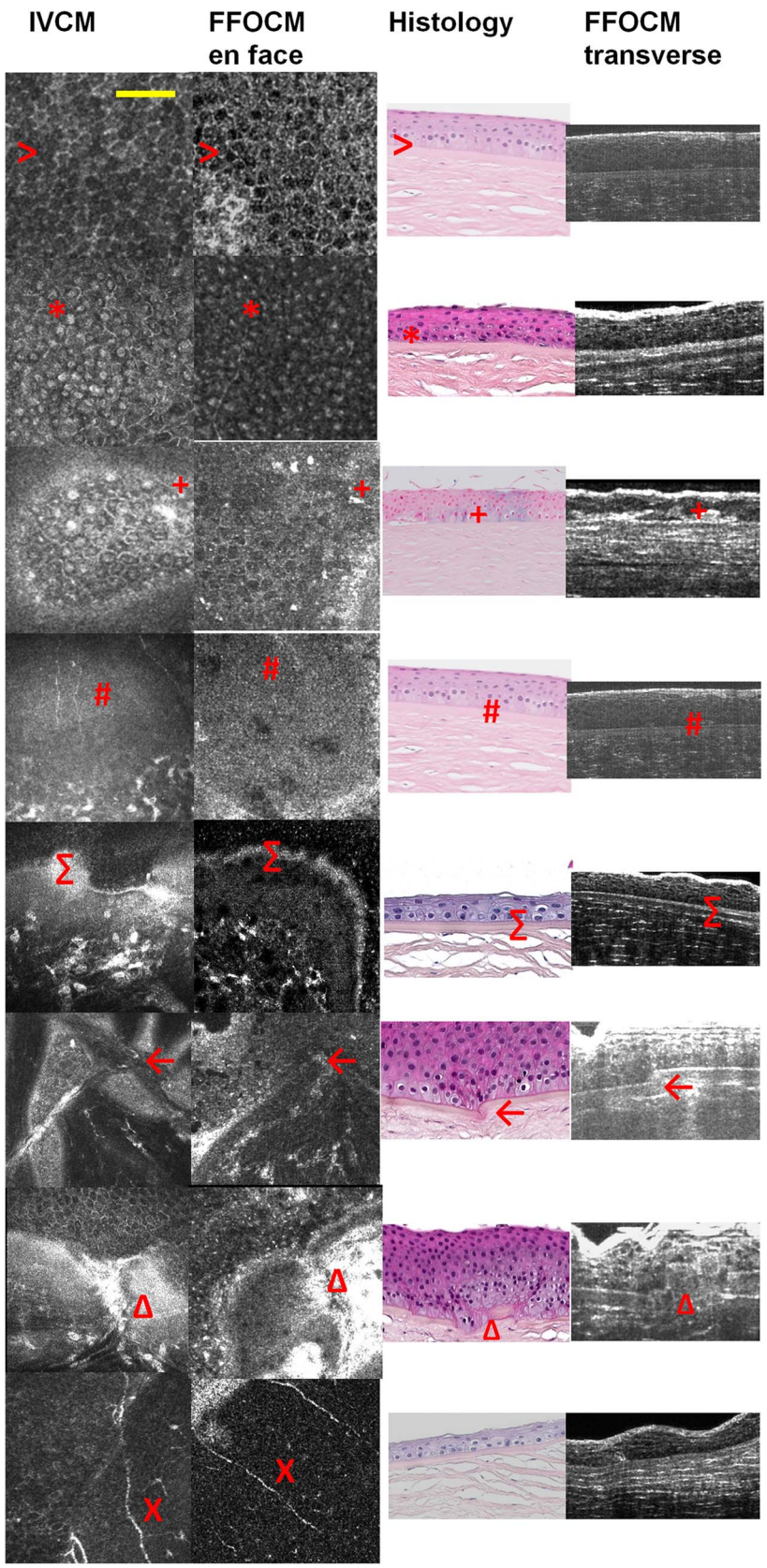

FIGURE 2. Epithelial and BL indicators of keratoconus. Scale bar 100 μm. En face views with IVCM (far left column) and FFOCM (center left column), and cross-sectional views in histology (center right column) and FFOCM (far right column). Indicators noted are as follows: >normal epithelial cells without visible nuclei; *flattened epithelial cells in keratoconus with visible nuclei; +ferritin deposits; #normal BL; ∑thickened hyperreflective basement membrane; ←BL kink; ΔBL rupture; Xsubbasal nerves visible en face only.

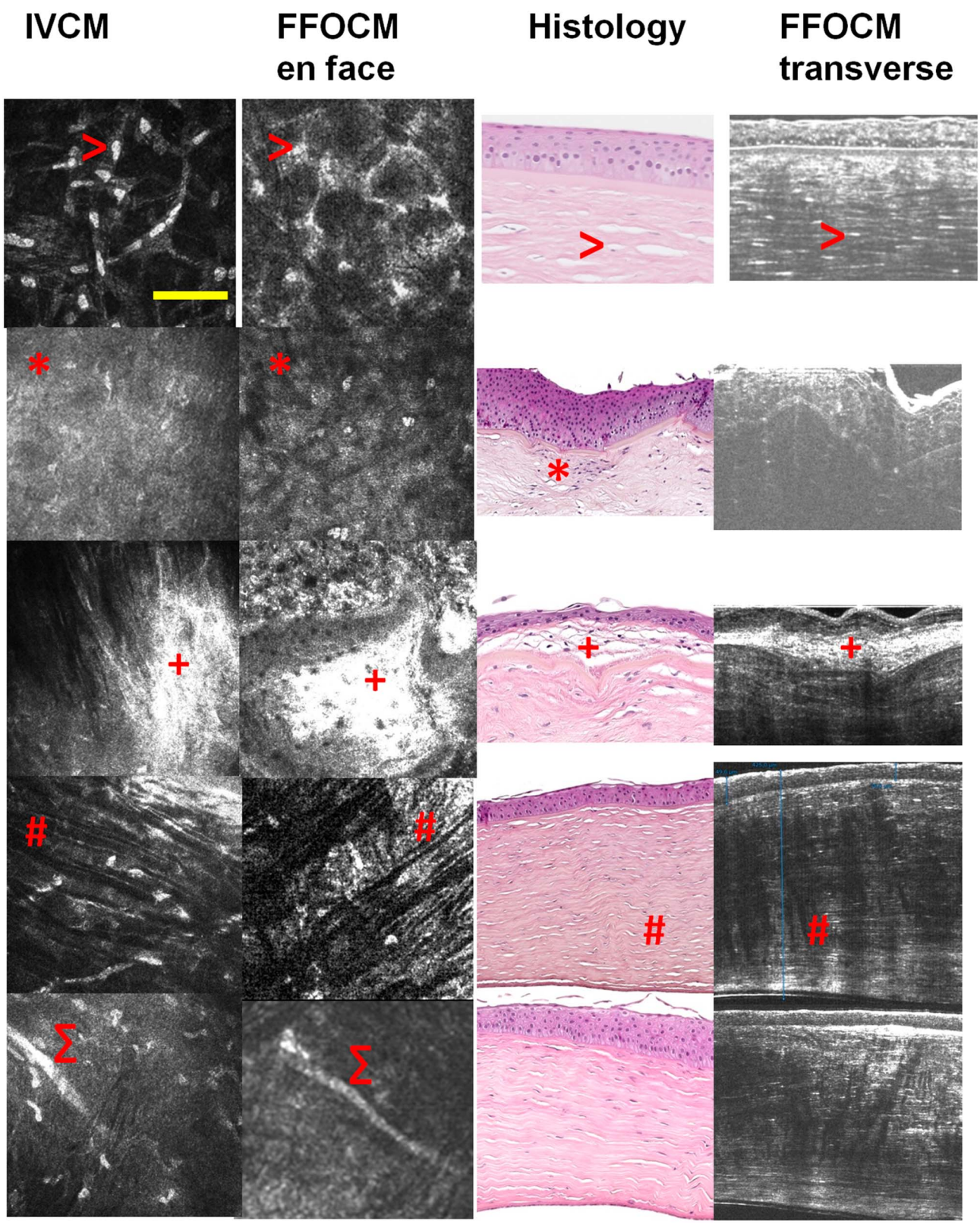

FIGURE 3. Stromal indicators of keratoconus. Scale bar 100 μm. En face views with IVCM (far left column) and FFOCM (center left column), and cross-sectional views in histology (center right column) and FFOCM (far right column). Indicators noted are as follows: >normal keratocytes in normal stroma; *hyperreflective haze; +subepithelial fibrosis; #Vogt striae; ∑stromal nerves visible en face only.

TABLE 3. Number of Indicators Seen in Each Modality and Comparison With Gold-Standard Histology

Indicator	No. Detected in Histology	No. Detected in FFOCM	No. Detected in SD-OCT	No. Detected in IVCM	No. Detected in SD-OCT Plus IVCM
Localized epithelial thinning	13	13	12	10	12
Localized epithelial thickening	10	13	11	8	11
Elongated superficial epithelial cells	13	10	—	5	5
Flattened basal epithelial cells	8	7	—	10	10
Ferritin deposits in the basal epithelial cell layer	9	12	—	6	6
Anomalies of the epithelial basement membrane	9	12	5*	10	10
Anomalous appearance of the subbasal nerve plexus	—	2	—	2	2
BL thinning	12	10	—	—	—
BL ruptures	10	9	—	—	—
BL region scarring	9	9	—	6	6
BL interruptions	8	3	—	—	—
Modifications of anterior stroma	7	10	10	8	10
Modifications of mid stroma	0	6	7	6	7
Vogt striae visible	10	13	3	11	11
Total no. finds	118	129	48	82	90

*Indicates that this indicator corresponds to anomalies at the basement membrane—BL region in SD-OCT (as these are not resolved with this technology).

224 ± 122 μm for keratoconus, so generally in mid stroma). The number of branches within the image field, and the thickness of nerves at 5 points in the field was measured for each subject, and the mean and SD of these values were compared and checked for significance (Table 4).

Statistical Analysis

A 2-tailed independent Student *t* test was used to compare variables, with a *P* value <0.05 considered as statistically significant.

TABLE 4. Cell Density Assessment of Keratoconus Versus Normal Cornea With IVCM

	Keratoconus	Normal Cornea	*P* (ANOVA)
Superficial epithelial cells, cells/mm^2	1738 ± 715	1339 ± 341	0.2
Wing cells, cells/mm^2	3696 ± 1246	4917 ± 1718	0.08
Basal epithelial cells, cells/mm^2	6174 ± 1821	8361 ± 2015	0.0007*
Keratocytes: overall stroma, cells/mm^2	245 ± 68	386 ± 88	<0.0001*
Very anterior stroma, cells/mm^2	349 ± 108	657 ± 145	<0.0001*
Anterior stroma, cells/mm^2	254 ± 51	401 ± 61	<0.0001*
Mid stroma, cells/mm^2	218 ± 48	364 ± 43	<0.0001*
Posterior stroma, cells/mm^2	199 ± 37	356 ± 64	<0.0001*
Endothelium, cells/mm^2	2803 ± 649	3303 ± 719	0.06
No. subbasal nerve branches	4 ± 4	3 ± 2	0.35
Thickness of subbasal nerves, μm	3 ± 1	3 ± 1	0.53
Thickness of stromal nerves, μm	9 ± 4	5 ± 3	0.01*

*Indicates significance.

RESULTS

Description of Indicators Seen in Keratoconus

Epithelium and BL

The epithelium of keratoconic corneas presented some or all of the following characteristics: localized epithelial thinning (Fig. 1), epithelial thickening in the region of maximal stromal thinning (Fig. 1), elongated superficial epithelial cells (Fig. 2, seen in HES histology and FFOCM cross-section as a flattened, detaching surface layer in cross-section), flattened basal epithelial cells (Fig 2, seen in HES histology, IVCM, and FFOCM en face views as enlarged cells with central rather than anteriorly positioned nuclei, in comparison with normal basal cells of Fig. 2), hyperreflective ferritin deposits in the basal epithelial cell layer (Fig. 2, hyperreflective in FFOCM and IVCM; requiring Perls' Prussian blue stain to be revealed in histology), and basement membrane abnormalities such as thickness variations and interruptions (Fig. 2, hyperreflective in FFOCM and IVCM; requiring periodic acid–Schiff staining to be revealed in histology).

Where normal cornea has a hyporeflective uniform thickness BL (Fig. 2), keratoconus damage in BL included regional thickness variations (Fig. 1), kinks (an abrupt change in BL direction within an otherwise continuous BL) (Fig. 2), ruptures (ie, a small discontinuity in BL, of similar size to a kink) (Fig. 2), interruptions/focal absences (ie, larger discontinuities in BL) (Fig. 1), and scarring (Fig. 1). The subbasal nerve plexus was visible at the basal epithelial cell layer in IVCM and FFOCM (Fig. 2). Subbasal nerves in keratoconus corneas appeared tortuous when compared with normal corneas, although the mean branch number was not significantly different (Table 4).

Stroma

Normal stroma is transparent with regularly distributed keratocytes (Figs. 1, 3), whereas transparency and regularity are disturbed in keratoconus. Modifications of anterior, mid, or posterior stroma, corresponding to newly formed connective tissue and/or haze, were seen with all modalities, although this aspect was particularly visible with SD-OCT and FFOCM where fibrous tissue appears hyperreflective (Figs. 1, 3). In histology, haze was defined as zones of increased keratocyte nuclear density. Vogt striae were observed with all modalities as diagonal criss-crossing bands in a complex 3D structure (Figs. 1, 3) with apparent anchor points to Bowman alterations (kinks, ruptures, and interruptions). Stromal nerves, seen in IVCM and FFOCM (Fig. 3), were significantly thicker in the keratoconus group than those in the normal group (Table 4, $P = 0.01$). Stromal thinning was observed only with SD-OCT because of the small number of penetrating keratoplasty cases observed.

Comparison of Imaging Modalities in Keratoconus Diagnosis

Comparison with gold-standard histology for each feature is evaluated in Table 3. FFOCM detected additional features to histology and did not suffer from fixation and slicing artifacts because it was performed on fresh tissue. As for in vivo modalities, SD-OCT detected 41% of those features visible in histology, and IVCM 69%. Because of complementarities of SD-OCT's transverse and IVCM's en face cellular resolution views, and their use for in vivo clinical imaging, it also seemed pertinent to evaluate the combination of SD-OCT and IVCM. Thus, the combination of SD-OCT plus IVCM enabled detection of 76% of features detected with histology.

Corneal cell Density Assessment

Cell densities assessed with IVCM are shown in Table 4. Basal epithelial cell density was significantly lower in the keratoconus group than that in the normal group ($P = 0.0007$). For all stromal layers, keratocyte density was significantly lower in the keratoconus group than that in the normal group ($P < 0.0001$). There were no significant differences in endothelial cell density between the keratoconus group and normal group.

Tissue Damage Due to Handling

For keratoconic corneas, detachment and/or rupture of the epithelium was observed in 50% of corneas with IVCM, 40% of corneas with FFOCM, and 0% with SD-OCT. For histology, to remove any effects of handling from other imaging modalities, histological sections of keratoconus corneas that had not been part of this study were selected at random from the hospital pathology archives. Epithelial detachments from the stroma and/or ruptures were detected in 100% of histological slices of n = 15 archived keratoconus corneas. No epithelial detachment was observed with any imaging modality on the healthy subject or donor cornea.

DISCUSSION

Strengths of Each Imaging Modality in Characterization of Keratoconus

With the various imaging modalities, our series of keratoconic corneas showed dramatic changes in the epithelium and its basement membrane, BL modification, decreased keratocyte density in accordance with the literature,[22–25] and stromal thinning and scarring. It should be noted that the study design did not allow early cases to be considered, as it included only surgical cases that correspond to advanced keratoconus in eyes where contact lens correction was no longer successful.

Several indicators of keratoconus found in this study have been previously described using SD-OCT including changes in corneal epithelial thickness, that is, thinning at the corneal apex and in the thinnest corneal zone, decreased inferior and thinnest epithelial thickness, and increased variability.[26–28] Corneal thinning, inferior displacement of the thinnest point, hyperreflective anomalies occurring at the BL level and in the stroma, and posterior displacement of the anterior hyperreflective structures are other SD-OCT indicators of keratoconus.[4,5] Pachymetric indices can be combined with SD-OCT to improve keratoconus detection.[29] SD-OCT is useful for evaluating the risk of hydrops in keratoconus, where increased risk of hydrops is indicated by increased epithelial thickening combined with stromal thinning at the conus, presence of hyperreflectivity at BL, and absence of stromal scarring.[30] In brief, Fuentes et al[30] showed that in a retrospective cohort of 191 advanced keratoconus cases, 11 cases of hydrops occurred during a mean follow-up of 30 months. Patients who presented acute keratoconus were young male patients with stage 3A keratoconus according to the SD-OCT classification, that is, the keratoconic cornea with pronounced stromal thinning and epithelial thickening, and stromal hyperreflectivities. Tissue changes seen on SD-OCT images in Figure 1, in particular stromal reflectivity abnormalities, could be best interpreted on comparison with FFOCM high-resolution cross-sections.

Indicators of keratoconus have been reported using IVCM including decreased basal epithelial cell and anterior and posterior stromal keratocyte densities, subbasal nerve fiber density, nerve branch density, and nerve fiber length; increased stromal nerve diameter; and Vogt striae.[22–24,31,32] In addition, the decline in keratocyte density has been shown to correlate with disease severity.[24,25] By carefully comparing IVCM images with images from SD-OCT, FFOCM, and histology, we were able to improve our 3D understanding of the tissue and better interpret the IVCM data, allowing us to identify features illustrated in Figures 1–3, such as flattened basal epithelial cells, hyperreflective ferritin deposits in basal epithelial cells, damage to basement membrane and BL, and stromal scarring in IVCM images.

BL thinning in the inferior corneal zone has been reported as an indicator of keratoconus using custom ultrahigh-resolution OCT.[33] In a similar fashion, FFOCM, due to its superior resolution compared with SD-OCT, enables detection of further indicators of keratoconus such as morphological changes in the basement membrane and BL (eg, basement membrane thickness

variations and interruptions, BL regional thickness variations, kinks, ruptures, interruptions/focal absences, and scarring).

Histology Artifacts on Ex Vivo Tissue

Epithelial detachments from stroma and/or ruptures were frequently seen in histological sections of keratoconus corneas. This seems to indicate that most damage to the fragile epithelium occurs during histological processing, and that this artifact may be avoided using other imaging modalities. In addition, lamellar dissociation seen in the stroma with histology was not seen with FFOCM. Thickness measurements with FFOCM therefore seem to be closer to reality than measurements from histological sections because FFOCM can be performed directly on fresh unmodified tissue.

It should be noted nevertheless that artifacts from histological processing, such as epithelial detachment and lamellar dissociation, do not necessarily impair accurate diagnosis.

CONCLUSIONS

Placido and/or Scheimpflug image-based corneal topography is accepted as the pragmatic, if not gold standard, in keratoconus diagnosis and quantification of progressive shape change. Effects on corneal shape and visual function are key in keratoconus patient management and assessment of interventions. However, studies on changes in the corneal structure by histopathology and imaging may help us understand keratoconus pathogenesis and perhaps characterize patient subsets. Using multiple imaging modalities, we were able to demonstrate that an almost equivalent number of diagnostic indicators of keratoconus are detectable in vivo by combining data provided by SD-OCT and IVCM, or ex vivo with FFOCM, to those detected by histopathology. More indicators could be found with ex vivo FFOCM than with the combination of in vivo SD-OCT and IVCM. Histology performed best for epithelial cell assessment, and FFOCM performed best for detection of stromal structure and changes in epithelial thickness. Histology requires multiple stains to reveal some indicators that were directly visible on the IVCM and FFOCM images and takes far longer to produce the images required for diagnosis. For clinical practice, SD-OCT with scans centered on the conus region combined with IVCM images taken in the same region from the superficial epithelial cell layer down to the endothelium can detect most indicators and provide almost as precise a diagnosis of keratoconus as histopathology.

ACKNOWLEDGMENTS

The authors thank Céline de Sousa for help with cell counting and histological processing.

REFERENCES

1. Krachmer JH, Feder RS, Belin MW. Keratoconus and related noninflammatory corneal thinning disorders. *Surv Ophthalmol.* 1984;28:293–322.
2. Rabinowitz YS. Keratoconus. *Surv Ophthalmol.* 1998;42:297–319.
3. Li X, Yang H, Rabinowitz YS. Keratoconus: classification scheme based on videokeratography and clinical signs. *J Cataract Refract Surg.* 2009;35:1597–1603.
4. Sandali O, El Sanharawi M, Temstet C, et al. Fourier-domain optical coherence tomography imaging in keratoconus: a corneal structural classification. *Ophthalmology*. 2013;120:2403–2412.
5. Li Y, Meisler DM, Tang M, et al. Keratoconus diagnosis with optical coherence tomography pachymetry mapping. *Ophthalmology*. 2008;115:2159–2166.
6. Efron N, Hollingsworth JG. New perspectives on keratoconus as revealed by corneal confocal microscopy. *Clin Exp Optom.* 2008;91:34–55.
7. Huang D, Swanson EA, Lin CP, et al. Optical coherence tomography. *Science*. 1991;254:1178–1181.
8. Yadav R, Kottaiyan R, Ahmad K, et al. Epithelium and Bowman's layer thickness and light scatter in keratoconic cornea evaluated using ultrahigh resolution optical coherence tomography. *J Biomed Opt.* 2012;17:116010.
9. Yadav R, Lee KS, Rolland JP, et al. Micrometer axial resolution OCT for corneal imaging. *Biomed Opt Exp.* 2011;2:3037–3046.
10. Petroll WM, Weaver M, Vaidya S, et al. Quantitative 3-dimensional corneal imaging in vivo using a modified HRT-RCM confocal microscope. *Cornea*. 2013;32:e36–e43.
11. Beaurepaire E, Boccara AC, Lebec M, et al. Full-field optical coherence microscopy. *Opt Lett.* 1998;23:244–246.
12. Dubois A, Vabre L, Boccara AC, et al. High-resolution full-field optical coherence tomography with a Linnik microscope. *Appl Opt.* 2002;41:805–812.
13. Ghouali W, Grieve K, Bellefqih S, et al. Full-field optical coherence tomography of human donor and pathological corneas. *Curr Eye Res.* 2015;40:526–534.
14. Akiba M, Maeda N, Yumikake K, et al. Ultrahigh-resolution imaging of human donor cornea using full-field optical coherence tomography. *J Biomed Opt.* 2007;12:041202.
15. Grieve K, Ghoubay D, Georgeon C, et al. Three-dimensional structure of the mammalian limbal stem cell niche. *Exp Eye Res.* 2015;140:75–84.
16. Grieve K, Paques M, Dubois A, et al. Ocular tissue imaging using ultrahigh-resolution, full-field optical coherence tomography. *Invest Ophthalmol Vis Sci.* 2004;45:4126–4131.
17. Borderie V, Martinache C, Sabolic V, et al. Light microscopic evaluation of human donor corneal stroma during organ culture. *Acta Ophthalmol Scand.* 1998;76:154–157.
18. Møller-Pederson T. A comparative study of human corneal keratocyte and endothelial cell density during aging. *Cornea*. 1997;16:333–338.
19. Optovue. Product sheet optovue. Available at: http://optovue.com/products/rtvue/. Accessed March 24, 2016.
20. Heidelberg Engineering. Product sheet HRTII. Available at: http://www.heidelbergengineering.com/us/products/hrt-glaucoma-module/cornea-module/. Accessed March 24, 2016.
21. Doughty MJ, Muller A, Zaman ML. Assessment of the reliability of human corneal endothelial cell-density estimates using a noncontact specular microscope. *Cornea*. 2000;19:148–158.
22. Ozgurhan EB, Kara N, Yildirim A, et al. Evaluation of corneal microstructure in keratoconus: a confocal microscopy study. *Am J Ophthalmol.* 2013;156:885–893.
23. Erie JC, Patel SV, McLaren JW, et al. Keratocyte density in keratoconus. A confocal microscopy study(a). *Am J Ophthalmol.* 2002;134:689–695.
24. Niederer RL, Perumal D, Sherwin T, et al. Laser scanning in vivo confocal microscopy reveals reduced innervation and reduction in cell density in all layers of the keratoconic cornea. *Invest Ophthalmol Vis Sci.* 2008;49:2964–2970.
25. Ku JY, Niederer RL, Patel DV, et al. Laser scanning in vivo confocal analysis of keratocyte density in keratoconus. *Ophthalmology*. 2008;115:845–850.
26. Temstet C, Sandali O, Bouheraoua N, et al. Corneal epithelial thickness mapping using Fourier-domain optical coherence tomography for detection of forme fruste keratoconus. *J Cataract Refract Surg.* 2015;41:812–820.
27. Li Y, Tan O, Brass R, et al. Corneal epithelial thickness mapping by Fourier-domain optical coherence tomography in normal and keratoconic eyes. *Ophthalmology*. 2012;119:2425–2433.
28. Rocha KM, Perez-Straziota CE, Stulting RD, et al. SD-OCT analysis of regional epithelial thickness profiles in keratoconus, postoperative corneal ectasia, and normal eyes. *J Refract Surg.* 2013;29:173–179.

29. Qin B, Chen S, Brass R, et al. Keratoconus diagnosis with optical coherence tomography-based pachymetric scoring system. *J Cataract Refract Surg.* 2013;39:1864–1871.
30. Fuentes E, Sandali O, El Sanharawi M, et al. Anatomic predictive factors of acute corneal hydrops in keratoconus: an optical coherence tomography study. *Ophthalmology*. 2015;122:1653–1659.
31. Bitirgen G, Ozkagnici A, Malik RA, et al. Evaluation of contact lens-induced changes in keratoconic corneas using in vivo confocal microscopy. *Invest Ophthalmol Vis Sci.* 2013;54: 5385–5391.
32. Hollingsworth JG, Efron N. Observations of banding patterns (Vogt striae) in keratoconus: a confocal microscopy study. *Cornea*. 2005;24: 162–166.
33. Abou Shousha M, Perez VL, Fraga Santini Canto AP, et al. The use of Bowman's layer vertical topographic thickness map in the diagnosis of keratoconus. *Ophthalmology*. 2014;121:988–993.